Indian Journal of Pure & Applied Physics
Vol. 60, September 2022, pp. 734-741
DOI: 10.56042/ijpap.v60i9.62495

Investigation of Synthesis Methods and Dope Type Effect on Conductivity and Luminescence Properties for CeO_2 Compounds

Handan Ozlu Torun[a*], Rabia Kırkgecit[b], Fatma Kilic Dokan[c] & Esra Ozturk[d]

[a*]Department of Energy System Engineering, Kahramanmaraş İstiklal University, Kahramanmaraş, 46300, Turkey

[b]Institute of Science, Material Science and Engineering, Kahramanmaraş Sütçü İmam University Kahramanmaraş, 46050, Turkey

[c]Department of Chemistry Processing Technologies, Kayseri University, Kayseri, Turkey

[d]Department of Metallurgical and Materials Engineering, Karamanoglu Mehmetbey University Karaman, Turkey

Received 20 April 2022; accepted 17 August 2022

The aim of this study is to investigate how the materials synthesized by both methods affect the luminescence and electrical properties. Also, another purpose is to examine the effect of doping types on optics and conductivity. At the end of the synthesis, X-Ray diffractometer (XRD) was used to examine the crystal structure and the possible different phases that may occur, Raman spectroscopy analysis was used to obtain information about the symmetry properties of the formed structure and the appearance of different vibration modes and the degradation (defect) formed in the structure. Photoluminescence (PL) Spectroscopy measurements at room temperature were employed. The peaks in the excitation spectrum at approximately 446 nm ($^5I_8 \rightarrow {}^5G_6$) correspond to the 4f-5d transition of the Ce^{3+} ion. Specific surface area analysis was performed using Brunauer-Emmett-Teller (BET). FE-SEM image was taken for morphological analysis of the structure. The ionic conductivity of the pelletized powder ceramic undoped CeO_2 and La^{3+}, and Ho^{3+} doped CeO_2 electrolyte was measured by impedance spectroscopy. The temperature value of the $Ce_{0.85}La_{0.10}Ho_{0.05}O_2$ sample synthesized by the high conductivity hydrothermal method was found as $5.64x10^{-3}$ $\Omega.cm^{-1}$ at 750 with the best conductivity result.

Keywords: Rare earth dope; CeO_2; Ionic conductivity; Luminescence

1 Indroduction

Advances in materials science are quite fast and remarkable. Functional nanomaterials have become important. It is especially important that a material is cheap, its toxicity is low and the variety of its application area is wide. In materials science, CeO_2 (cerium oxide) is an oxidized compound with cubic fluorite crystal lattice, wide band gap and 4f orbitals[1,2]. Due to this feature, it has many application areas. For example, i) ceramic electrolyte in solid oxide fuel cells[3], ii) antibacterial in biochemistry[4], iii) catalytic converter in automotive industry[5], v) photocatalysis in wastewater disposal[6] vi) optoelectronic devices[7]. In addition, doping of rare earth elements into CeO_2 provides the expansion and efficiency of the mentioned applications. For example, in photoluminescence studies, CeO_2 containing rare earth elements absorbs strong light and transfers it from oxygen ions to Ce^{4+} ions[8,9]. It shows a characteristic emission feature according to the structure of the rare thoracic element that acts as an activator. It is seen that RE-doped CeO_2 compounds with red, orange and green emissions in litters are used in imaging devices[10-12]. In solid oxide fuel cells, the electrolyte used as ceramic electrolyte is desired to have high ionic conductivity and low operating temperature[13]. The ionic conductivity of pure CeO_2 compound is low. Furthermore, the reduction of Ce^{4+} / Ce^{3+} at the operating temperature of the fuel cell creates an unstable structure. It is known that rare earth elements contribute to the CeO_2 structure in order to increase conductivity and provide stability[14,15].

The crystalline structural properties of the compounds obtained in both fields of application are important. The crystalline properties may vary according to the synthesis methods of the compounds[16]. The low crystal size of the compounds obtained after the synthesis method can increase the efficiency. Different methods such as sol-gel[17], hydrothermal[18], polymer pyrolysis method[19], microwave[20], solid-state method[21] are used to obtain the CeO_2 and CeO_2 compounds.

*Corresponding authors:
(Email: handan.ozlutorun@istiklal.edu.tr)

In this study, the conductivity and optical properties of (La,Ho) doped CeO_2 compounds, which have hardly been studied in the literature, were investigated.(La,Ho) co-doped CeO_2 compound was synthesized by both sol-gel method and hydrothermal method. Also, the effect of synthesis methods on the conductivity and emission characteristics of the compounds obtained was investigated.

2 Materials and Methods

2.1. Powder synthesis

Undoped CeO_2 and $Ce_{0.85}La_{0.10}$ $Ho_{0.05}O_2$ compounds were synthesized by both sol-gel and hydrothermal methods. In both synthesis reactions, cerium (III) nitrate hexahydrate (Ce $(NO_3)_3.6H_2O$), lanthanum (III) nitrate hexahydrate (La $(NO_3)_3.6H_2O$), holmium (III) nitrate pentahydrate (Ho $(NO_3)_3.5H_2O$) were used as starting compounds. In the sol-gel method, the starting compounds, which were weighed in a stoichiometric ratio, were dissolved in pure water. Citric acid and ethylene glycol were added to it and it waited for gel consistency at 80 °C. The gel-like sample was dried at 120 °C for 12 hours. It was ground and heat-treated at 800 °C for 12 hours. In the hydrothermal method, the starting compounds were dissolved in pure water and 6 M NaOH solution was added dropwise. The creamy mixture was placed in an autoclave in a teflon container. Reaction conditions were set at 180 °C for 12 hours. The filtered sample was washed with alcohol and distilled water. The samples dried at room temperature were ground and heat-treated at 800 °C for 12 hours.

2.2. Materials Characterization

The crystal properties of the synthesized photocatalysts were examined X-Ray Diffraction Method (XRD, Pananalytic Imperial). XRD pattern measurements of all samples were made using a 0.02° step angle in the range of 2θ = 10-90°, at 40 kV and 40 mA. XRD powder pattern was indexed using Diffrac Plus, Win-Metric programs, and unit cell parameters were calculated. The surface morphology of compounds was investigated by Field Scanning Electron Microscope (FE-SEM, Zeiss). BET (Brunauer– Emmett–Teller) surface area measurements were characterized via N_2 adsorption/ desorption measurements (mmicrometric Gemini IV). Raman (WITec alpha 300 M^+) measurements were taken to check the bonding structures and binding of synthesized samples. Raman measurements were made using a 532 nm wavelength laser. Measurements were taken at 3 mW laser power. Impedance spectroscopy was used in conductivity studies of the compounds obtained. Optical properties were examined with a Fluorescence spectrophotometer (HITACHI F-7100) All PL measurements were performed in an open atmosphere and at room temperature.

3 Results and Discussion

3.1. XRD analysis

The XRD pattern of samples is given in Fig.1.The crystal size of the compounds was calculated from the XRD powder pattern using the Debye-Scherrer formula, which is given with Eq 1.

$$D = \frac{0.94\lambda}{\beta.cos\theta} \quad (1)$$

Where λ is the wavelength of the x-ray, θ X-ray diffraction angle, and β is the width of the half-peakheight in radians. The half-peak height width (FWHM) value β was calculated from the XRD pattern using the Topas program. The lattice parameters (a = b=c) of the cubic system are calculated using to the Miller indices (hkl) and the interplanar spacing. The interplanar spacing (d) is obtained from Bragg's law. In the calculations, peaks in the (111) (220) (311) plane were used. The change in crystal size is due to the different synthesis method. Crystal structure parameters are shown in Table 1. The change in unit cell parameters of La-Ho doped compounds is related to the ionic radii of the dope elements. It has pure CeO_2 cubic crystal lattice. During the synthesis reaction, some Ce^{4+} ions in the crystal structure are replaced by dope elements. As a

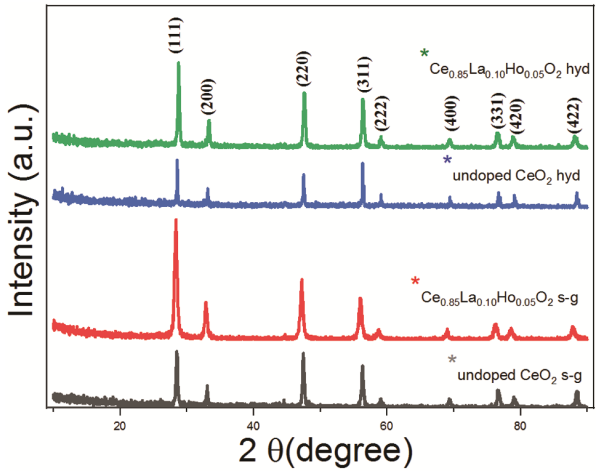

Fig. 1 — X-ray diffraction pattern of undoped CeO_2 and $Ce_{0.85}La_{0.1}Ho_{0.05}O_2$ powder synthesized by sol-gel and hydrothermal methods.

Table 1 — Crystal structure properties.

Samples	Lattice parameters a (Å)	Space Group	Volume (Å)^3	Crystalline size (nm) Mean value	(111)	(022)	(113)
Undoped CeO_2 (hyd)	5.4127	Fm-3m	158.58	53.77	76.48	26.84	27.99
$Ce_{0.85}La_{0.10}Ho_{0.05}O_2$ (hyd)	5.4518	Fm-3m	161.31	22.36	25.36	22.21	17.98
Undoped CeO_2 (s-g)	5.4159	Fm-3m	158.86	29.76	32.18	26.84	27.98
$Ce_{0.85}La_{0.10}Ho_{0.05}O_2$(s-g)	5.4400	Fm-3m	160.96	21.45	17.89	22.17	23.09

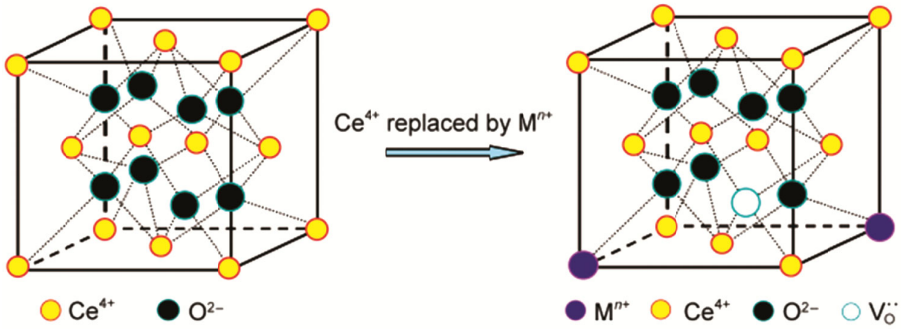

Fig. 2 — Crystal structure of undoped CeO_2 and doped CeO_2.

result, the main crystal structure is preserved and oxygen vacancy are formed. Elements placed in the lattice change the unit cell size. The ionic radii of the elements are Ce 0.967 Å, La^{3+} 1.15 Å, Ho^{3+} 0.894 Å, respectively[22]. Since the radii of La^{3+} and Ho^{3+} ions are larger than Ce^{4+}, an increase in unit cell size has been observed.

Oxygen hole formed in the crystal structure are shown by the KörngVing equation[23].

$$La_2O_3 + Ho_2O_3 + 2Ce_x + 4O_x \longrightarrow 2LaCe^{+} + 2HoCe^{+} + VO.. + 2\,CeO_2 \quad \ldots (2)$$

The rare earth elements dope in the Eq.2. and as shown in the Fig. 2 are replaced by Ce^{4+} ions. And after the reaction, oxygen ion hole are formed. It deals with the properties of dope types from changes in the lattice structure.

As can be seen in Table 1, although the synthesis method is different, the cubic phase was obtained. However, the cubic crystal lattice parameters were changed. The sol-gel method reduced crystal size.

3.2. Raman Spectroscopy Analysis

Raman spectroscopy is a branch of vibrational spectroscopy used in the evaluation of trace amounts of samples as structural and sensitive. It provides useful information about changes in the crystal structure. Raman analyzes of the samples were performed at room temperature, taken from several points. All spectra of the samples are shown in

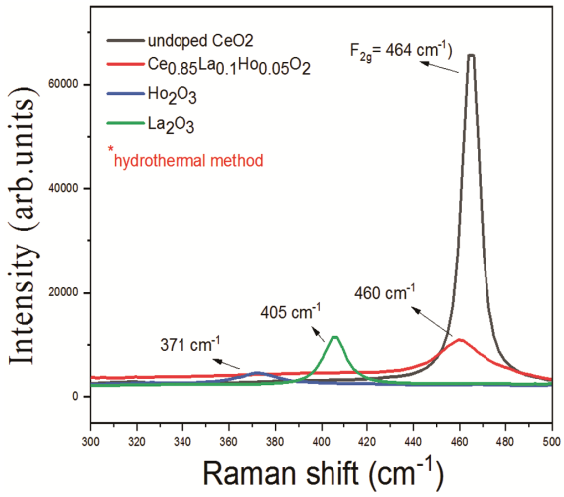

Fig. 3 — Raman spectra of undoped CeO_2 and La^{3+}, Ho^{3+} doped CeO_2 samples synthesized by hydrothermal method.

Fig. 3-4. It shows a 462 cm^{1-} peak in the undoped CeO_2 Raman spectrum. This shows the CeO_2, fluorite cubic F_{2g} Raman active mode and belongs to the Ce-O8 symbol. In Raman studies, it belongs to the CeO_2 structure with the characteristic fluorite cubic structure, F3m space group, approximately 440-465cm^{-1} peak[24,25]. As can be seen, the La_2O_3 and Ho_2O_3 Raman spectra used in the doping yielded peaks at different points. However, the Raman spectra of the compounds obtained after the doping process are compatible with the CeO_2 structure. It confirms that the additive elements are stabilized with Ce^{4+} in

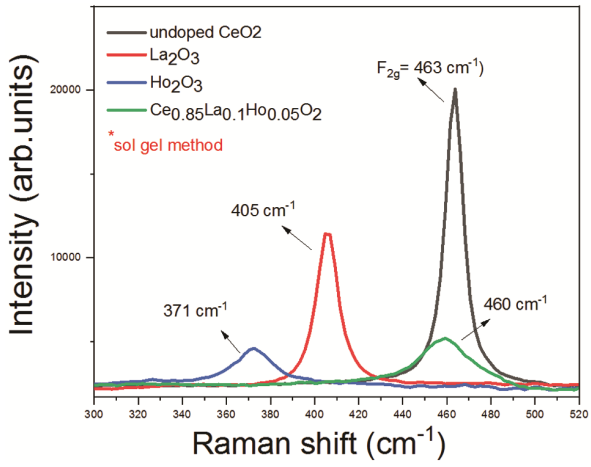

Fig. 4 — Raman spectra of undoped CeO_2 and La^{3+}, Ho^{3+} doped CeO_2 samples synthesized by sol-gel method.

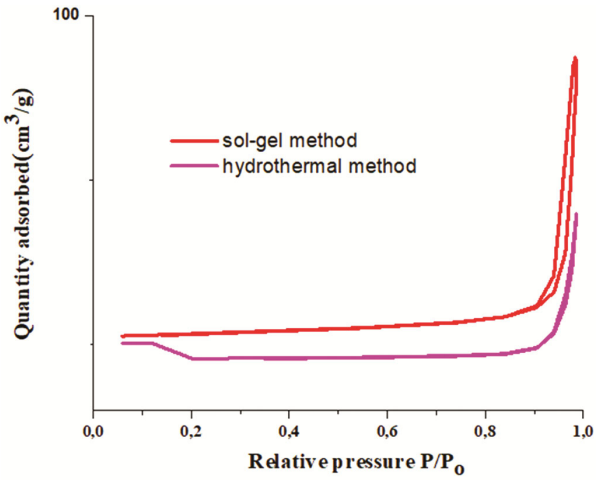

Fig. 5 — Nitrogen adsorption-desorption isotherms of La^{3+}, Ho^{3+} doped CeO_2 samples.

crystalline structure. Results are in line with XRD assessments.

The shift in the F2g value in both synthesis methods may indicate that an oxygen gap is formed in the structure[18].

3.3. BET Analysis

BET analysis was performed to determine the surface area properties of undoped CeO_2 and La^{3+}, Ho^{3+} doped CeO_2 samples synthesized by hydrothermal and sol-gel methods. The specific surface area was estimated by applying the Brunauer -Emmett-Teller (BET) equation to the experimental N_2 isotherm using a micrometric-Gemini IV analyzer. 30 mg of each sample was degasificated for 24 h at 250 °C, and nitrogen adsorption-desorption isotherm was analyzed through the BET method. Fig. 5. shows the adsorption-desorption isotherms of the samples. The curve is like the type 3 isotherm curve in the IUPAC definition [26]. The adsorption isotherms of the first layer are defined as type 3 adsorption heat, which is smaller than the heat of condensation, and capillary condensation is less. Adsorption isotherms in solids with very low adsorption power are suitable for this type.

While the surface area of the compound produced by sol-gel was 11.9290 m²/g, it was found to be 4.1219 m² / g in hydrothermal. The surface area of the compound synthesized with sol-gel was larger. Compared to the crystal size change obtained from XRD, the results support each other**.**

3.4. Oxide İon Conductivity Measurement (Impedance spectrum)

Conductivity behaviors of the samples were examined with an impedance analyzer. Samples synthesized by both methods were pressed before conductivity measurement and sintered at 1350 ℃ for 12 hours. Sintered disc shaped samples were dyed with silver paste to ensure good contact before impedance measurements. It was dried at 100 °C. For the measurement of each sample, 50 up to 400, after 400, it was terminated with 750 ℃ temperature increase with 25 temperature increase. In the measurements, data were taken in the frequency range of 100 kHz-100 mHz. As software, a test program was created with Power Sine software in the PowerSuit program. When the conductivity graphs were examined, it was observed that the grain and grain boundary resistances of undoped CeO_2 sol-gel, hydrothermal undoped CeO_2 and sol-gel La-Ho samples were formed. The conductivity of the CeO_2 ceramic electrolyte depends on the dope type and amount, microstructure, sintering temperature and time[27].In the hydrothermal La-Ho sample, only garin resistance occurred. Conductivity values of the synthesized samples are given in Table 2. It has been found that the conductivity value of undoped CeO_2 is low for both methods. It is expected that undoped CeO_2 conductivity is low compared to doping[28]. In order to examine the relationship between conductivity and grain, the surface morphology of pelleted samples was examined after conductivity measurement. As can be seen in Fig. 6(a-c), the grains are not fully formed at the temperature at which the conductivity is measured at 500. Unwanted porosity in the structure is high. This situation causes the total resistance to increase. With doping and increasing conductivity measurement temperature, both grain

Table 2 — Conductivity results of samples.

Samples	Methods	Calcination Temperature(°C))	Conductivity (750 °C) (Ω.cm-1)m^{-1})
Undoped CeO_2	Sol-gel	1350 °C, 12h	$8.44x10^{-10}$
	Hydrothermal	1350 °C, 12h	$2.07x10^{-10}$
$Ce_{0.85}La_{0.10}Ho_{0.05}O_2$	Sol-gel	1350 °C, 12 h	$2.31x10^{-11}$
	Hydrothermal	1350 °C, 12 h	$5.64x10^{-3}$

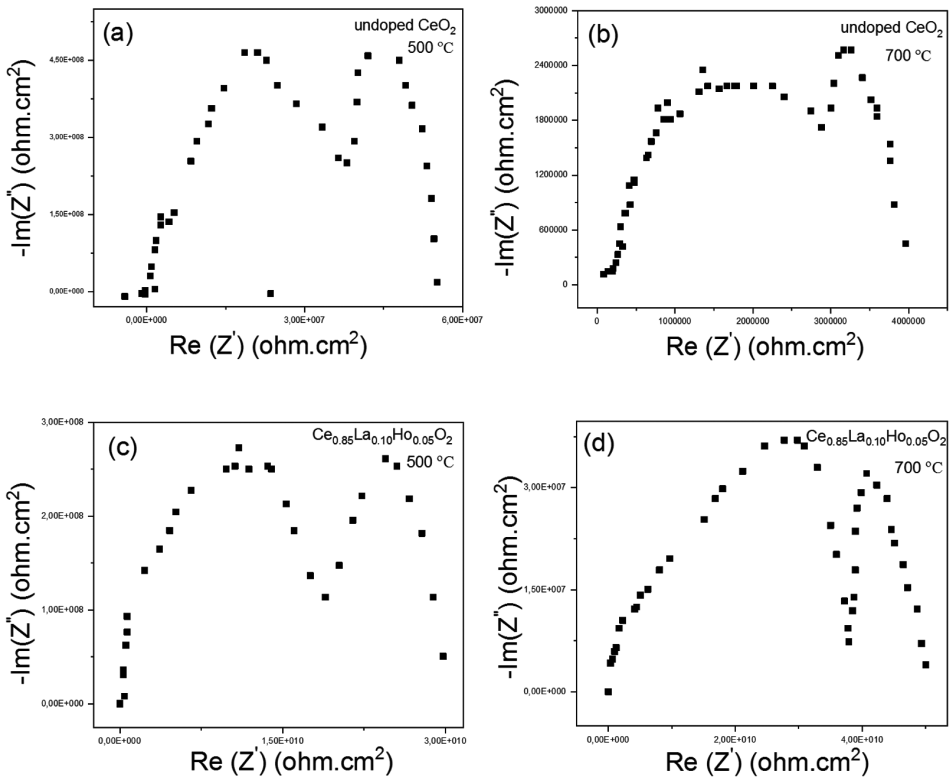

Fig. 6 — Nyquist curves of pure CeO_2 and La^{3+}, calcined at 1350°C, synthesized by sol-gel method, and Ho^{3+} doped CeO_2 at 500-700°C conductivity temperature.

and grain boundary conductivity were observed Fig. 6(b-d). Since the grain and grain boundary resistance effect decreased, the conductivity increased.

When we examine Fig. 7(a), it is seen that undoped CeO_2 has high resistance and low conductivity caused by excess porosity at a conductivity temperature of 500. Both grain and grain boundary show conductivity. However, with the increase in conductivity temperature, the resistance decreased with the decrease of porosity in the structure Fig. 7(b). As La, Ho doping and conductivity increase the oxygen space, the resistance decreased Fig. 7(c). The increase in the conductivity temperature increased the conductivity. Compared to the hydrothermal method sol-gel method, the size and structure of the formed grains decreased the grain boundary resistance and increased the total conductivity .

Also, their conductivity behavior can be evaluated by the crystal properties given in Table 2. The crystal size and lattice parameters of La-Ho doped wrist synthesized by hydrothermal method are large. Compared to the sol-gel compound, the movement of oxygen ions in the crystalline structure becomes easier and the resistance decreases.

When the conductivity results were evaluated, it was expected that the sol-gel method had a positive effect, but the opposite was true. One reason for this is that the high grain boundary resistance decreased the total conductivity. In addition, when the surface images of the compound produced by hydrothermal synthesis after 1350 ^oC sintering are examined, pores are seen. The porous structure may cause electronic conductivity to contribute to total conductivity.

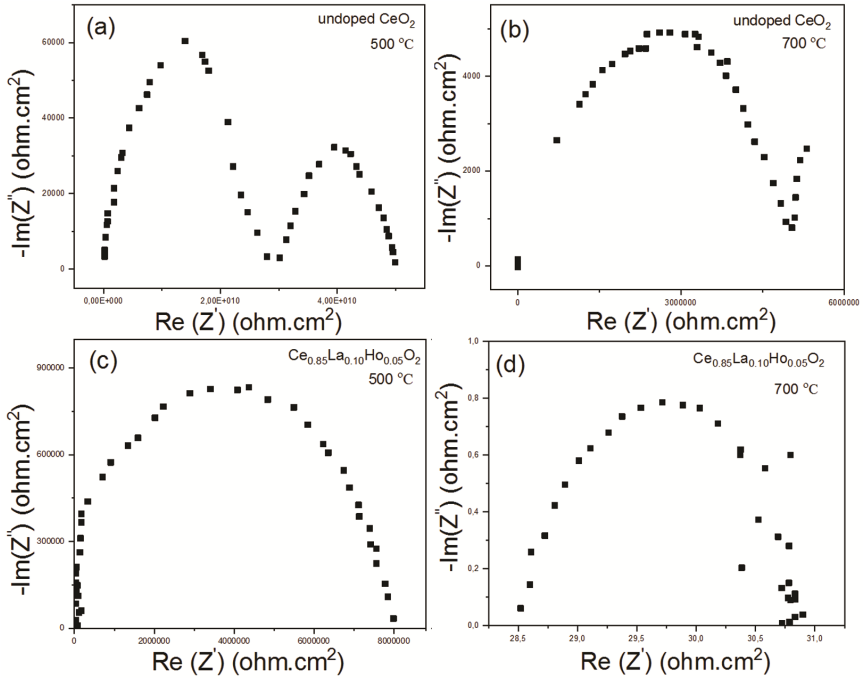

Fig. 7 — Nyquist curves of pure CeO_2 and La^{3+}, calcined at 1350°C, synthesized by hydrothermal method, and Ho^{3+} doped CeO_2 at 500-700°C conductivity temperature.

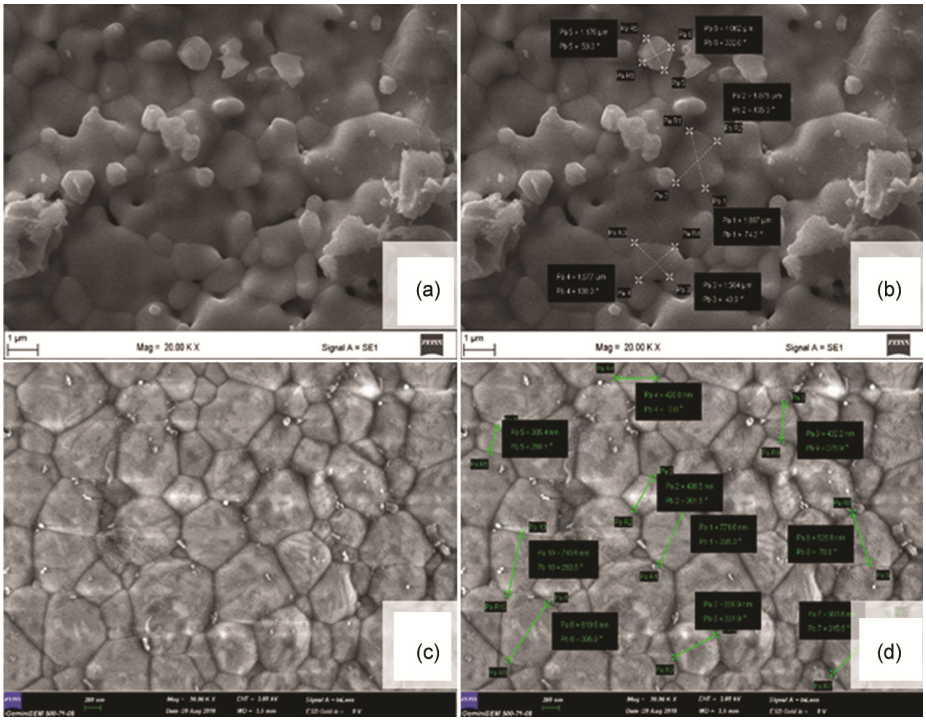

Fig. 8 — FE-SEM images of samples synthesized by sol-gel method a-b) undoped CeO_2, c-d) $Ce_{0.85}La_{0.1}Ho_{0.05}O_2$.

3.5. Microstructures (FE-SEM)

The FE-SEM technique was used to observe the micro and morphological structure properties of the sample and to determine the distribution of the grains. After the impedance analysis of pure CeO_2 and $Ce_{0.85}La_{0.1}Ho_{0.05}O_2$ powder sample synthesized by sol-gel and hydrothermal method, FE-SEM images are shown with density and grain. As seen in Fig 8 & 9,

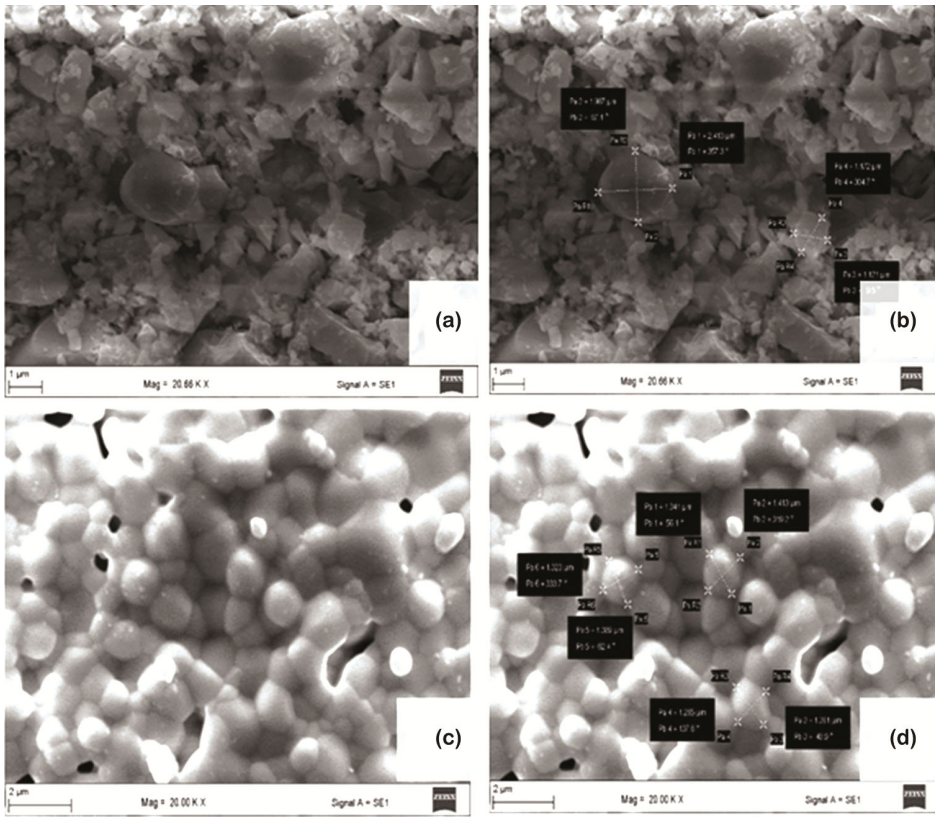

Fig. 9 — FE-SEM images of samples synthesized by hydrothermal method a-b) undoped CeO_2, c-d) $Ce_{0.85}La_{0.1}Ho_{0.05}O_2$.

the particles show a more homogeneous distribution after sol-gel synthesis. The porosity is quite low.

3.6. Photoluminescence (PL) studies

The excitation and emission spectra of La^{3+}, Ho^{3+}doped CeO_2samples synthesized by sol-gel and hydrothermal method is shown in Fig .10. The excitation bands centered at ~300 nm and ~438 nm were observed in the samples under 538 nm emission. The excitation band at 300 nm is originated from the charge transfer band (CTB). The excitation band at 438 nm can be attributed to the transition from $^5I_8$ state to the $^5G_6$ states of Ho^{3+}ions. Additionally, Fig. 10 shows the room temperature emission spectra of the La^{3+} and Ho^{3+} ions doped CeO_2 phosphors synthesized by sol-gel and hydrothermal method under a 438 nm excitation. Both samples exhibit intense green and relatively weak near-infrared emission bands, which are originated from the $^5S_2 \rightarrow {}^5I_8$ transition (~538 nm) and crystal defects emission (~800 nm), respectively[29-30]. In Fig. 10, the excitation and emission bands of La^{3+} ions were not observed. Thus, it can be said that most of the excitation energy is captured Ho^{3+}ions. In other

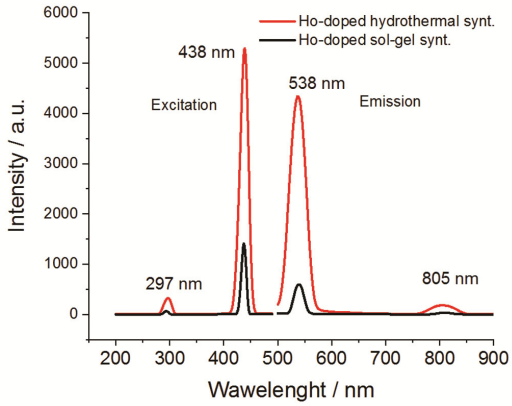

Fig. 10 — Excitation and emission spectra of La^{3+}, Ho^{3+}doped CeO_2samples synthesized by sol-gel and hydrothermal method.

words, there is no energy transfer between La^{3+} ions and Ho^{3+} ions. In addition, when the excitation and emission intensities of the samples synthesized by the sol-gel method and hydrothermal method are compared, it is seen that the luminescence intensity of the sample synthesized by the hydrothermal method is higher than the other. In this case, we can say that the hydrothermal method gives better luminescence intensity for $La^{3+}$and Ho^{3+} co-doped CeO_2.

4 Conclusions

In this study, cubic phase compounds were obtained with both methods. The crystals of the compounds obtained by the sol-gel method were smaller in size and the surface area was larger. At the selected sintering temperature, the diffusion rate was insufficient in the compound obtained by the hydrothermal method and pores were formed. The high total conductivity results for the hydrothermal method may have been due to the contribution of the porous structure to the electronic conductivity. Also in this study, the excitation and emission spectra of La^{3+}, Ho^{3+} doped CeO_2 samples synthesized by sol-gel and hydrothermal method are compared. For both samples, the excitation bands centered at ~300 nm and ~438 nm and the $^5S_2 \rightarrow {}^5I_8$ (~538 nm) and crystal defects (~800 nm) emission bands were observed. Although both phosphors have same luminescence spectra, the luminescence intensity of La^{3+} and Ho^{3+} doped CeO_2 samples synthesized by the hydrothermal method is higher than the other phosphor. Such luminescent materials can be used for optoelectronic applications where mainly green emission is desired.

Acknowledgment

This work was supported by Kahramanmaraş Sütçü İmam University (Project No: 2019/5-7 YLS).We would like to thank Niğde Nejat Veziroğlu Clean Energy Research Center for their support in the conductivity studies.

References

1 Kaviyarasu K, Fuku X, Mola G T, Manikandan E, Kennedy J & Maaza M, *Mater Lett*, 183 (2016) 351.
2 Kumar P, Kumar P, Kumar A, Meena R C, Tomar R, Chand F, & Asokan K, *J Alloys Compd*, 672 (2016) 543.
3 Torun H O & Çakar S, *J Thermal Anal Calorime*, 133 (2018) 1233.
4 Bakkiyaraj R, Balakrishnan M, Bharath G & Ponpandian N, *J Alloys Compd*, 724 (2017) 555.
5 Di M R, Fornasiero P, Graziani M & Kašpar J, *J Alloys Compd*, 275 (1998) 877.
6 Gnanasekaran L, Hemamalini R, Saravanan R, Ravichandran K, Gracia F, Agarwal S, & Gupta V K, *J Photochem Photobiol B: Biol*, 173 (2017) 43.
7 Kumari K, Aljawfi R N, Chawla A K, Kumar R, Alvi P A, Alshoaibi A & Kumar S, *Ceram Int*, 46 (2020) 7482.
8 Malleshappa J, Nagabhushana H, Prasad B D, Sharma S C, Vidya Y S & Anantharaju K S, *Optik*, 127 (2016) 855.
9 Sudarshan K, Tiwari V, Utpalla P & Gupta S K *Inorg Chem Front*, 6 (2019) 2167.
10 Jeyanthi C E, Siddheswaran R, Medlín R, Chinnu M K, Jayavel R & Rajarajan K *J Alloys Compd*, 614 (2014) 118.
11 Carvalho L G, Rocha L A, Buarque J M, Gonçalves R R, Nascimento C S, Schiavon, M A & Ferrari J L, *J Lumin*, 159 (2015) 223.
12 Basavaraj R B, Navami D, Deepthi N H, Venkataravanappa M, Lokesh R, Kumar, K S & Sreelakshmi T K, *Inorg Chem Commun*, 120 (2020) 108164.
13 Abdalla A M, Hossain S, Azad A T, Petra P M I, Begum F, Eriksson S G & Azad A K *Renew Sustain Energy Rev*, 82 (2018) 353.
14 Kobi S, Jaiswal N, Kumar D & Parkash O, *J Alloys Compd*, 658 (2016) 513.
15 Eressa L A & Rao P B, *Mater Chem Phys*, 242 (2020) 121914.
16 Kim G, Lee N, Kim K B, Kim B K, Chang H, Song S J & Park J Y, *Int J Hydrogen Energy*, 38 (2013) 1571.
17 Kirkgeçit R & Torun H Ö, *Process Appl Ceram*, 14 (2020) 314.
18 Mendiuk O, Nawrocki M & Kepinski L, *Ceram Int*, 42 (2016) 1998.
19 Swatsitang E, Phokha S, Hunpratub S & Maensiri S, *Physica B: Condens Matter*, 485 (2016) 14.
20 Prado-Gonjal J, Heuguet R, Muñoz-Gil D, Rivera-Calzada A, Marinel S, Morán E & Schmidt R, *Int J Hydro Energy*, 40 (2015) 15640.
21 Ishida T, Iguchi F, Sato K, Hashida T & Yugami H, *Solid State Ionics*, 176 (2005) 2417.
22 Shannon R D & Prewitt C D, *Acta Crystallog*, 25 (1969) 925.
23 Cesário M R, Savary E, Marinel S, Raveau B & Caignaert V, *Solid State Ionics*, 294 (2016) 67.
24 Singh K, Kumar K, Srivastava S & Chowdhury A, *Ceram Int*, 43 (2017) 17041.
25 Li M, Zhang R, Zhang H, Feng W & Liu X, *Micro Nano Lett*, 5 (2010) 95.
26 Sing K S W, Everett D H, Haul R A W, Moscou L, Pierotti R A, Rouquerol J & Siemieniewska T, *Pure Appl Chem*, 57 (1985) 603.
27 Wang Y, Mori T, Li J G & Drennan J, *J Europ Ceram Soc*, 25 (2005) 949.
28 Ramesh S, Raju, K J & Reddy C V, *Trans Nonferrous Metals Soc China*, 24 (2014) 393.
29 Wang X, Bu Y, Xiao S, Yang X & Ding J W, *Appl Phys B*, 93 (2008) 801.
30 Chen G Y, Yang G H, Aghahadi B, Liang H J, Liu Y, Li L & Zhang Z G, *J Opt Soc Am B,* 27 (2010) 1158.